Fabrication and Electrochemical Characterization of Micro- and Nanoelectrode Arrays for Sensor Applications

Nur Azura Mohd Said,[a,b] Karen Twomey,[a] Vladimir I. Ogurtsov,[a] Damien W.M. Arrigan,[c] Grégoire Herzog[a]

[a]:Tyndall National Institute, Lee Maltings, University College Cork, Cork, Ireland
[b]:Biotechnology Research Centre, Malaysian Agricultural Research & Development Institute, Serdang, Selangor, Malaysia
[c]: Nanochemistry Research Institute, Department of Chemistry, Curtin University, Perth, Australia
gregoire.herzog@tyndall.ie

Abstract. This paper describes the fabrication of microelectrode arrays, with two different geometries: disc (Designs d1 and d2) and band (Designs b1, b2 and b3) using three critical dimensions (100 nm, 1 µm and 10 µm) leading to 5 different designs, fabricated by the combination of UV photolithographic and e-beam lithographic techniques. Three silicon nitride layer thicknesses (200, 300 and 500 nm) were chosen to determine an optimized transducer design and fabrication process. Cyclic voltammetry characterisation using a simple redox probe ion, ferreocenecarboxylic acid in phosphate buffered saline electrolyte solution, demonstrated steady-state voltammetric curves for d1, d2, b1 and b2. A good agreement between experimental and theoretical data is found for devices d1, d2, b1 and b2. The experimental current for b3, on the other hand, is much lower compared to the calculated one- perhaps due to the overlapping of the diffusion layers of neighbouring microelectrodes in the array.

1. Introduction

Microelectrode arrays are gaining popularity in recent decades, particularly in electroanalytical chemistry. Nevertheless, historically, the greatest drive towards the early development of solid microelectrodes has arose in the 1940s and 1950s when the need to measure oxygen concentrations in living biological organisms became of paramount importance [1] with the first tungsten microelectrode fabricated over 50 years ago by the 1981's Nobel Laureate David H. Hubel[2]. IUPAC has outlined that a microelectrode has dimensions of tens of micrometers or less, down to submicrometer range[3] whilst nanoelectrode is defined as an electrode having dimensions on the order of a few tens of nanometres[4]. Due to their small sizes, microelectrodes offer a series of advantages compared with the conventional macroelectrodes including: (i) enhanced rates of mass-transport, (ii) decreased ohmic drop and (iii) increased signal-to-noise ratio. As a result of these characteristics improved response time, greater sensitivity with limits of detection down to sub-parts per billion and improved response are achieved[5]. The drawbacks of the use of single microelectrodes, however, are that they produced low current output and are more susceptible to mains interference[6,7]. These can be overcome with the use of arrays of microelectrodes, whereby multiple microelectrodes are operated in parallel. According to Arrigan[8], if collections of these electrodes are arranged in an ordered manner with a controlled inter-electrode

spacing, they are referred to as arrays; and if the collections are not so ordered and there is no specific control over the inter-electrode spacing, then they are referred to as ensembles. In terms of microelectrode arrays fabrication techniques, Huang et al. (2009)[9] has described mainly five techniques which include: i) assembly techniques (e.g random assemblies of micro-wires[7]); ii) photolithography (thin film fabrication by the deposition of metallic film, namely Ag, Pt, Au and Ir, on Si_3N_4 or silicon oxides layer[5,10,11]) ; iii) screen-printing technique (for mass production and cheaper regular disk arrays[12]); iv) direct electrodeposition; and v) modification of the microelectrode array (molecular modification on the array surface, hydrophobic block, patterned electrodeposition, and pattern-based carbon nanotube/nanofiber microarrays). Apart from that, other techniques reported are the focused ion beam milling for the fabrication of recessed nanoband electrodes[6] and nanopore array electrodes[13], reactive-ion etching[14] and CMOS[15]. We report here the fabrication and the characterisation of electrode arrays, which will be used for the immobilisation of nanosome for the detection of odourants. Two different geometries for the nanotransducers have been selected: disc (Designs d1 and d2) and band (Designs b1, b2 and b3) using three critical dimensions for these structures (100 nm, 1 µm and 10 µm) leading to 5 different designs. Three silicon nitride layer thicknesses (200, 300 and 500 nm) were chosen to determine an optimized transducer design and fabrication process. The summary of the designs used in terms of their geometry and sizes are presented in Table 1.

Table 1 Summary of the five different types of transducers

Design	Geometry	Width/diameter	Length	N electrodes	Surface area/cm^2
d1	Disc	10 µm	-	314	2.466×10^{-4}
d2	Disc	1 µm	-	75	5.89×10^{-4}
b1	Band	10 µm	500 µm	17	8.5×10^{-4}
b2	Band	1 µm	50 µm	9	4.5×10^{-6}
b3	Band	100 nm	5 µm	75	3.75×10^{-7}

2. Materials and methods

2.1. Fabrication

The fabrication of the transducer device is a combination of UV photolithographic and e-beam lithographic methods to pattern electrodes with critical dimensions ranging from 100 nm to 10 microns. A silicon oxide layer is thermally grown on the silicon substrate and alignments marks are patterned on it. Titanium, platinum and gold layers are deposited by e-beam evaporation on the silicon wafer. The 20 nm thick titanium layer acts as an adhesion layer, which will improve the quality of the gold layer deposit. Silicon nitride is then deposited by plasma-enhanced chemical vapour deposition on the surface and will act as a passivation layer. Three silicon nitride layer thicknesses were selected: 200, 300 and 500 nm. Openings of the passivation layer are done in the silicon nitride by plasma etching to form the micro- and nanoelectrode arrays.

2.2 Electrochemistry set-up

The wafers were diced into individual chips (Figure 1). Five different designs of the transducer arrays were designed as described in Table 1. Disc and band arrays are described in Figure1B and 1C.

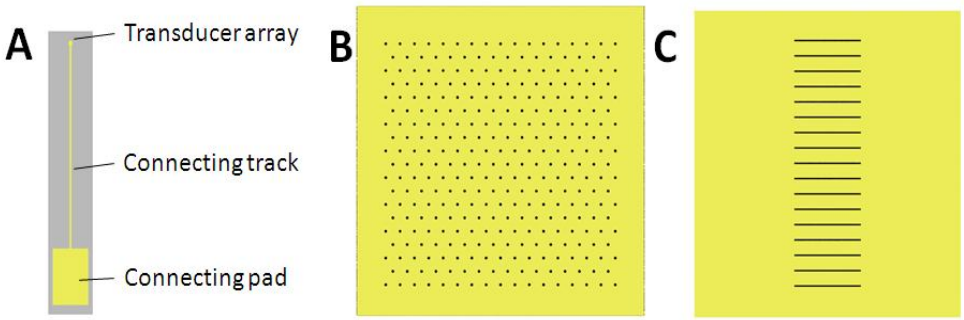

Figure 1: Schematic representation of the fabricated device and of the transducer array of (B) design d1 and (C) b1 layouts.

Prior to use, the nanotransducer devices are treated for 3-5 minutes in air plasma at 100 W, 600 mTorr (Harrick Plasma, New York, USA) to remove residual organic matter that may remain after the fabrication process. and were connected to the potentiostat using a custom made connector kindly provided by Uniscan Limited (Buxton, UK). The electrochemistry study was carried out with CHI660B potentiostat (CH instruments, IJ Cambria, Burry Port, Wales, United Kingdom) in 1 mM solution of ferrocenecarboxylic acid in PBS (0.01 M, pH7.4) using three electrochemical system with with a Ag | AgCl | 3 M KCl commercial reference electrode and a platinum wire commercial electrode. The devices fabricated are tested with cyclic voltammetry (CV) in a three electrode cell configuration at scan rate of 5, 10, 20, 50, 100, 200 and 500 mVs^{-1} over the potential range 0.1 to 0.6 V. All chemicals are obtained from Sigma-Aldrich and purified water with a resistivity of 18 MΩ cm, from an Option R50 system (Veolia Water Systems, Ireland).

3. RESULTS AND DISCUSSIONS

3.1 Visual characterisation of the transducer devices

Scanning electron and optical micrographs of the fabricated transducer devices were taken (Figure 2) and the dimensions were measured (Table 2).

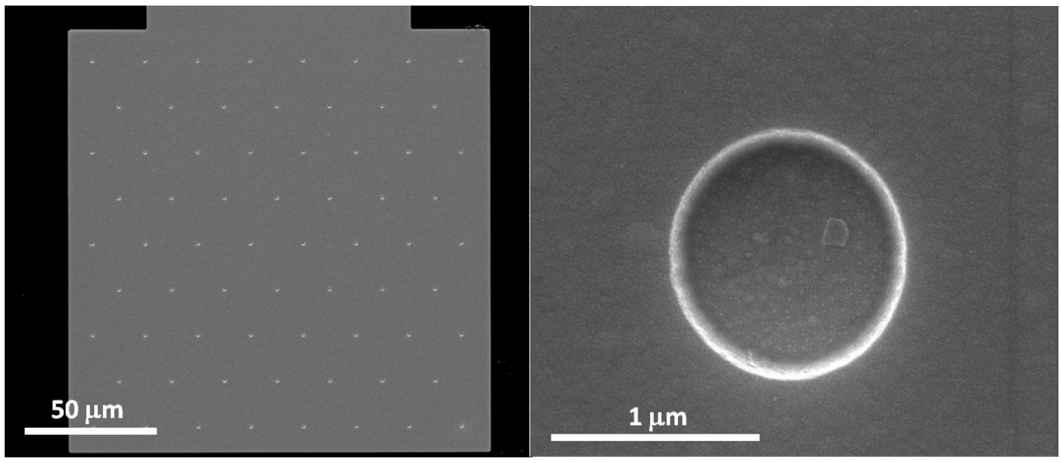

Figure 2: SEM images of design b2 full array (left) and of a single microelectrode (right)

Table 2: Expected and achieved critical dimensions for the transducer devices

		200 nm		300 nm		500 nm	
Design	**Critical dimension µm**	**Dimensions achieved µm**	**Relative error**	**Dimensions achieved µm**	**Relative error**	**Dimensions achieved µm**	**Relative error**
d1	10	9.31	-0.07	8.89	-0.11	8.89	-0.11
d2	1	1.168	0.17	1.236	0.24	0.964	-0.04
b1	10	9.52	-0.05	10.26	0.03	10.58	0.06
b2	1	1.195	0.19	1.297	0.30	1.03	0.03
b3	0.1	0.250	2.50	0.279	2.79	0.084	-0.16

The larger feature dimensions (d1 and b1) that were realised correspond to the expected with a 10% accuracy regardless of the silicon nitride thickness. However, for the smallest features (d2, b2 and b3), the dimensions achieved vary greatly with the thickness. Especially, it is inherent for silicon nitride thicknesses of 200 and 300 nm that there was no silicon oxide layer between the silicon nitride and the e-beam resist. For the 500 nm thick silicon nitride wafers the dimensions achieved were much closer to the expected dimensions compared to the wafers with thinner silicon nitride layers. The reason for the widening of the opening is due to the lack of selectivity of the etching process for silicon nitride over the e-beam resist.

3.1 Electrochemical characterisation of the transducer devices

The five different designs were characterised by CV and as expected, CV curves for d1, d2, b1 and b2 exhibited steady state shape peak at 100 mV s^{-1} (Figure 3). However CV for b3 is greatly dependant on the scan rate and exhibited peak shape at 10mV s^{-1}. The CV for b3 with different scan rates (not shown here) is similar as reported by Lanyon et al. (2007)[13] using 3 x 3 nanopore array with pore radii of 80 nm and the current obtained also were in the same range as ours (picoA). Berduque et al. (2007)[10] has employed Equation 1.1 and 1.2 for the calculation of theoretical limiting current for both recessed micro-disc electrodes and inlaid micro-band electrodes:

$$i_{\lim} = \left(\frac{4\pi nFCDr^2}{4L + \pi r} \right) N \qquad \text{Eq. 1.1}$$

$$i_{\lim} = \frac{2\pi nFCDL}{\ln\left(\frac{64\ Dt}{w^2} \right)} N \qquad \text{Eq. 1.2}$$

where D is diffusion coefficient (5.7×10^{-6} cm^2 s^{-1}), F is Faraday constant (96485 $Cmol^{-1}$), A is the surface area, r is the radius, L is the silicon nitride thickness (recess depth), w is the band electrode width, L is the band electrode length, C is the concentration of ferrocene carboxylic acid, t is the time of experiments and n is the number of electrons involved in the reaction.

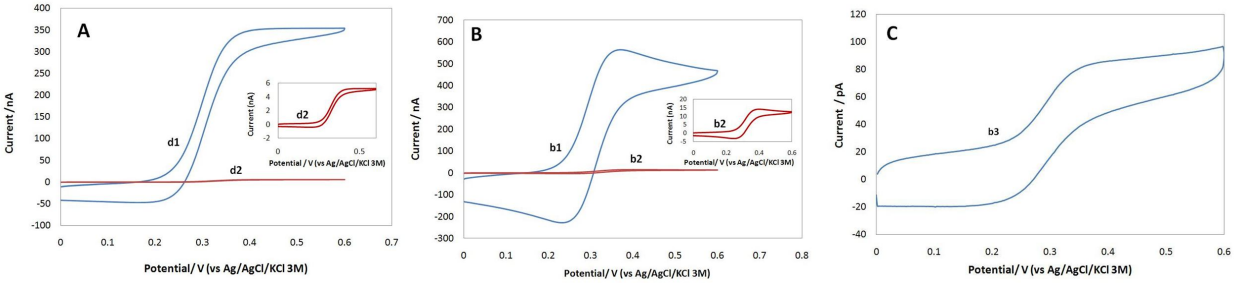

Figure 3: CV for d1 and d2 microdisc array (A); b1 and b2 microband array (B); both at 200 nm recess, scan rate 100mVs^{-1}; CV for microband array b3 at 200 nm recess with scan rate 10 mVs^{-1} (C)

A good agreement between experimental and theoretical data is found for devices d1, d2, b1 and b2, as shown in Table 3. However, the current measured for the nanotransducer device of b3 is 100 times lower than the one expected. Lanyon et al. (2007) also has obtained a lower experimental current compared to the calculated ones for the recessed nanobands used[6]. The decrease of the current might due to the overlapping of the diffusion layers of neighboring microelectrodes in an array hence the behaviour of the array becomes that of a macroelectrode and the voltammograms tail off due to planar diffusion[11,16]. Equation 1.2 also does not take into account the presence of the recess, which for the nanobands in this case, is larger than the critical dimension (width) of the electrode.

Table 3: Comparison between the theoretical current and experimental current for transducers

Design	L / nm	Theoretical current/ nA	Experimental current (nA)
d1	200	329	344 ± 5
	300	321	328 ± 5
	500	306	318 ± 12
d2	200	5.47	4.9 ± 0.3
	300	4.68	3.9 ± 0.6
	500	3.63	3.3 ± 0.7
b1	200	649	529 ± 7
	300		510 ± 28
	500		517 ± 16
b2	200	17	13 ± 0.3
	300		13 ± 2
	500		14 ± 5
b3	200	9.4	0.06 ± 0.002
	300		0.06 ± 0.003
	500		0.07± 0.001

The efficiency of the silicon nitride layer to prevent diffusion of ferrocenecarboxylic acid to diffuse and react at the underlying gold layer was verified by running CV at transducer devices with no opening in the silicon nitride layer. No faradaic current is recorded when there is no opening in the silicon nitride on the control designs (Figure 4).

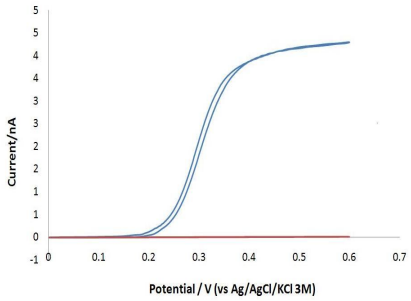

Figure 4: CV at transducer d2 with 314 discs of 1 micron in diameter (blue line) and with no opening in the silicon nitride (red line).

4. CONCLUSIONS

This paper has described the fabrication of microelectrode arrays of microdisk and microband with various recess depth using UV photolithographic and e-beam lithographic techniques. Both microdisk array (d1 and d2) and microband array (b1 and b2) was successfully characterized via visual images and electrochemical study. CV curves for d1, d2, b1 and b2 exhibited steady state shape peak at 100 mV s^{-1} and the experimental limiting current obtained are in the vicinity of the calculated theoretical current. For d3 nanoband, however, the CV shape is more inclined to peak/sigmoidal shape and the CV is greatly dependant with the scan rate. This micro- and nanoelectrode array will be used for the immobilisation of olfactory receptor for the sensing of odourants.

Acknowledgements:

The authors gratefully acknowledge the European Commission (Bioelectronic Olfactory Neuron Device, Grant agreement N° 228685) for support for this work and Malaysian Agricultural Research & Development Institute (MARDI) for the scholarship award.

References

(1) A.M. Bond, K.B. Oldham, C.G. Zoski, *Anal. Chim. Acta*, **1989**, *216*, 177.
(2) D.H. Hubel, *J. Psychiatr. Res.* **1971**, *8*, 301.
(3) K. Štulík, C. Amatore, K. Holub, V. Mareček, W. Kutner, *Pure Appl. Chem.* **2000**, *72*, 1483.
(4) R.G. Compton, G.G. Wildgoose, N.V. Rees, I. Streeter, R. Baron, *Chem. Phys. Lett.* **2008**, *459*, 1.
(5) V. Beni, D.W.M. Arrigan, *Current Anal. Chem.* **2008**, *4*, 229.
(6) Y.H. Lanyon, D.W.M. Arrigan, *Sens.Actuat. B: Chem.* **2007**, *121*, 341.
(7) S. Fletcher, M.D. Horne, *Electrochem. Commun.* **1999**, *1*, 502.
(8) D.W.M. Arrigan, *Analyst*, **2004**, *129*, 1157.
(9) X.J. Huang, A.M. O'Mahony, R G. Compton, *Small*, **2009**, *5*, 776.
(10) A. Berduque, Y.H. Lanyon, V. Beni, G. Herzog, Y.E. Watson, K. Rodgers, F. Stam, J. Alderman, D. W. M. Arrigan, *Talanta*, **2007**, *71*, 1022.
(11) N. Godino, X. Borrise, F.X. Munoz, F.J. del Campo, R.G. Compton, *J. Phys. Chem. C*, **2009**, *113*, 11119.
(12) O. Ordeig, F.J. del Campo, F.X. Munoz, C.E. Banks, R.G. Compton, *Electroanalysis* **2007**, *19*, 1973.
(13) Y.H. Lanyon, G. De Marzi, Y.E. Watson, A.J. Quinn, J.P. Gleeson, G. Redmond, D.W.M. Arrigan, *Anal. Chem.* **2007**, *79*, 3048.
(14) M.E. Sandison, N. Anicet, A. Glidle, J.M. Cooper, *Anal. Chem.* **2002**, *74*, 5717.
(15) R. Lenigk, H. Zhu, T.C. Lo, R. Renneberg, *Fres. J. Anal. Chem.* **1999**, *364*, 66.
(16) T.J. Davies, R.G. Compton, *J. Electroanal. Chem.* **2005**, *585*, 63.